Dalton Transactions

ROYAL SOCIETY OF CHEMISTRY

COMMUNICATION

View Article Online
View Journal | View Issue

Cite this: *Dalton Trans.*, 2025, **54**, 12766

Received 2nd July 2025,
Accepted 6th August 2025

DOI: 10.1039/d5dt01559f

rsc.li/dalton

Impact of the second coordination sphere of the molybdopterin cofactor on the mechanism of formate dehydrogenase from *Cupriavidus necator*

Matthew J. Kapelis and Jarett Wilcoxen *

Molybdenum containing enzymes play a pivotal role in the global carbon and nitrogen cycles using a common molybdopterin cofactor. Mechanistic studies have revealed a great deal about molybdenum enzymes but have yet to detail the impact the secondary binding interactions have on catalysis. Herein, we describe a double variant of formate dehydrogenase from *Cupriavidus necator* (*Cn*Fds) that changes the electrostatic and hydrogen bonding to the ligands to molybdenum resulting in a complete loss of formate oxidation activity, which occurs by outer sphere hydride transfer, and gain of nitrate reduction activity, which is proposed to follow an inner sphere oxygen atom transfer mechanism. We have assigned these observed changes to the stability of the terminal ligand which in turn directs the catalytic outcome. The results here illustrate the importance of the secondary sphere interactions in directing oxygen atom transfer *vs.* hydride transfer mechanisms in molybdenum containing enzymes.

Molybdenum (Mo) containing enzymes are widely distributed in nature playing integral roles in the global carbon, sulfur, and nitrogen cycles.[1] The largest and most diverse family of Mo-containing enzymes is the dimethylsulfoxide reductase (DMSOR) family.[2] In the DMSOR family, the Mo cofactor (MoPDT) is made up of two equivalents of a pyranopterin guanosine dinucleotide (PDT) which ligates Mo by the dithiolene moiety. Additionally, there is often a ligand from the peptide and a terminal oxo or sulfido ligand, Fig. 1. To accommodate the vast substrate scope catalyzed by members of the DMSOR family, the MoPDT is likely tuned *via* covalent and non-covalent interactions between the cofactor and peptide binding pocket. Primary and secondary sphere interactions within an enzyme active site can have profound effects on the reactions catalyzed by the enzyme, especially in enzymes that utilize metallocofactors.[3–7] In the case of Mo-containing enzymes, the roles of these secondary sphere interactions in modulating the reactivity of the metal site are poorly understood. X-ray crystal structure models of members of the DMSOR family have highlighted some of these differences with peptide-cofactor interactions that include direct ligation of the metal by a peptide residue such as cysteine, aspartate, or serine, hydrogen bonding to the PDT, including the dithiolene thiols, or electrostatic and/or π-stacking interactions with the planes of the PDT.[8–15]

The impact of the primary and secondary coordination sphere can be highlighted by two structurally related enzymes with fundamentally different reactivities, periplasmic nitrate

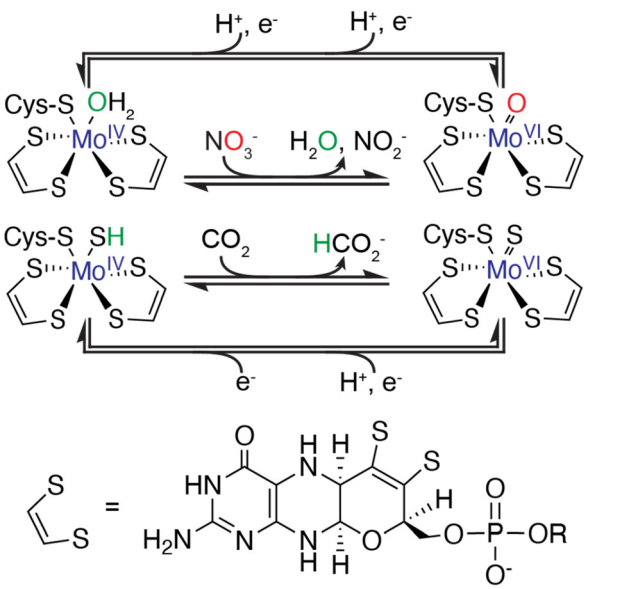

Fig. 1 Proposed mechanism for NapA (top) and formate dehydrogenase (bottom). NapA catalyzes an oxygen atom transfer mechanism where nitrate displaces a bound water and oxygen from nitrate is transferred to Mo followed by reduction of Mo and protonation of the terminal oxo.[21] Fdh follows a hydride transfer mechanism where the hydride is proposed to originate from the terminal sulfido ligand.[19] The structure of the pyranopterin dinucleotide has been simplified to the dithiolene moiety. The full lignad is shown with an "R" group that is typically guanosine bound through the phosphate group.

Department of Chemistry and Biochemistry, University of Wisconsin- Milwaukee, Milwaukee, WI 53211, USA. E-mail: Jarettw@uwm.edu

reductase (NapA) and formate dehydrogenase (Fdh). In general, Mo-containing enzymes typically catalyze oxygen atom transfer reactions to (or from) a variety of substrates.[1] This is not the case for Fdh which catalyzes an intrinsically different reaction, reversible hydride transfer between formate and the MoPDT to yield CO_2.[2,16–18] The hydride transfer mechanism requires a terminal sulfido in place of the terminal oxo typically found in the Mo coordination sphere DMSOR family, Fig. 1.[19,20] In contrast to the generally agreed upon mechanism and coordination sphere of Mo in Fdh, there has been considerable debate over the primary coordination environment and mechanism of NapA. Recent efforts investigating NapA from *Campylobacter jejuni* using a variety of spectroscopic and kinetic techniques have demonstrated a terminal oxo is found in the functional enzyme.[21–24] This difference in the terminal ligand, sulfido in the case of Fdh and oxo in the case of NapA, is likely a key feature that facilitates the very different reactivates observed in the respective enzymes.

Despite the different chemistries catalyzed by NapA and Fdh, the enzymes share a superimposable protein structure, Fig. SI1, a conserved [Fe_4S_4] cluster adjacent to the MoPDT, and share a nearly identical binding pocket for the MoPDT that includes many highly conserved residues that include hydrogen bond donors and acceptors, and aromatic π-stacking to the PDT ligands.[25,26] While not a substrate for Fdh, nitrate is commonly used as a protectant during purification to limit the inactivating effect of oxygen on the active site.[27] Nitrate, which is also a competitive inhibitor during formate oxidation, is thought to bind near the Mo center limiting oxygen access.[28] Phylogenetically, NapA is described as more closely related to formate dehydrogenase and arsenite oxidase than other DMSOR family members.[29] Recent work investigating variants to a conserved lysine in both NapA and Fdh impairs or inhibits catalysis depending on the variant.[22,30] The lysine hydrogen bonds one of the two pyranopterins and a conserved [Fe_4S_4] cluster that shuttles electrons to or from the MoPDT in both enzymes and is thought to affect the electron transfer between the two cofactors in a similar way. These similarities highlight that it is subtle differences between the two enzymes that stabilize a differentiated terminal ligand and the intrinsic mechanism catalyzed by these two enzymes.

Previous investigations of the residues in the secondary coordination sphere of Fdh from *Rhodobacter capsulatus* (*Rc*FdsDABG) identified three residues: His387Met, Arg597Thr, and a deletion of Arg^{597} that were able to impart nitrate reductase activity to *Rc*FdsDABG when changed to the corresponding residues in NapA.[25] His^{387} is likely to be involved in hydrogen bonding interactions with the Cys ligated to Mo, Fig. 2. Arg^{587} and Arg^{597} are located further away near the substrate access tunnel and likely orient the substrate or participate in transition state stabilization. Unfortunately, these variants also retained formate dehydrogenase activity resulting in an unclear model for what drives the stability of the terminal ligand (oxo or sulfido) that is necessary to drive the different reactivities. Here, we describe a double variant of formate dehydrogenase from *Cupriavidus necator* (*Cn*FdsDABG) which changes the intrinsic reactivity from a formate oxidation to a nitrate reduction with complete loss of detectable formate oxidation activity.

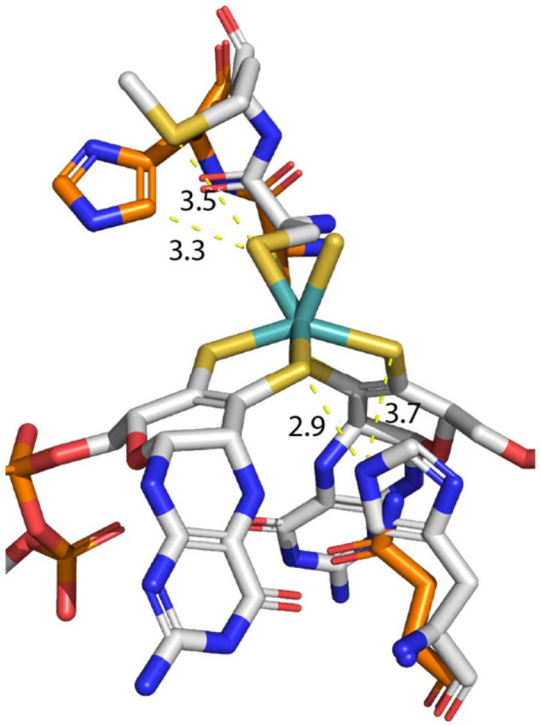

Fig. 2 Active site of *Rc*FdsA (PDB: 6TGA) in orange and NapA (PDB: 3ML1) in gray highlighting residues in this study. The residues are within hydrogen bonding distance of the ligating Cys (His and Met in FdsA and NapA respectively) or the thiol in the ligating proximal dithiolene (Asn and His in FdsA and NapA respectively). The structures were aligned in Pymol according to sequence and fold which resulted in with overlapping MoPDT, only the MoPDT from NapA is shown for clarity. Distances between residues and coordinating sulfurs are in angstroms.

While the secondary structure of NapA and Fdh are highly conserved there are a few residues that differ between Fdh and NapA but remain conserved within the two enzyme types. One of the residues discussed above, the His proximal to the ligating cysteine is highly conserved in Fdh while this residue is a highly conserved methionine in NapA, Fig. 2 and Fig. SI2. In *Cn*FdsDABG, His^{379} (equivalent to His^{387} in *R. capsulatus*) makes a hydrogen bond with the ligating Cys while the lone pair on the sulfur of the conserved Met of NapA points toward the cysteine sulfur in an electrostatic interaction, Fig. 2. A second residue that is highly conserved in NapA is a His that hydrogen bonds with one of the ligating dithiolene sulfurs of the proximal pyranopterin (relative to the conserved [Fe_4S_4] cluster), Fig. 2. In Fdh, the interacting residue is not strictly conserved but tends to be polar (glutamine, serine, or asparagine), suggesting an electrostatic interaction, likely from the ketone or alcohol oxygen of the residue. When both His^{379} and Asn^{827} in the FdsA subunit of *Cn*FdsDABG are changed to Met and His respectively, as is found in NapA, the enzyme loses its ability to oxidize formate with no apparent reaction when

using NAD+, benzyl viologen, or methyl viologen as an electron acceptor monitoring the reduction of the electron acceptors over several hours. Conversely, the enzyme is active in nitrate reduction when using methyl viologen cation radical (MV) as an electron donor. Steady-state assays monitoring the observed rate of MV oxidation against nitrate concentration can be fit with the Michaelis–Menten equation to yield a turnover rate (k_{cat}) of 0.68 s^{-1} and Michaelis constant (K_m) of 1.57 mM, Fig. 3. The reaction rate varies slightly with pH with a maximum near pH 8, similar to the optimum Fdhs and NapA, SI Fig. 3. We note dithionite (reduction potential of ~−400 to −600 mV) can act as an electron donor with a turnover rate monitoring the bleaching of the dithionite absorbance at 314 nm that is similar to MV (−446 mV) while assays monitoring the consumption of NADH (−320 mV) are active but ~10× slower.[31] Next, considering nitrate is an effective inhibitor in the wild-type enzyme against formate oxidation, we examined if formate could act as an inhibitor to the reduction of nitrate by varying the concentration of formate and nitrate. While we observe no significant effect on the overall rate with increasing formate concentrations, we observe a more pronounced impact on the K_m for nitrate which decreases in the presence of formate, Fig. 3, to approximately 0.3 mM suggesting cooperative binding. Further investigations to clarify the role of formate in this mechanism are ongoing.

As discussed above, previous investigations of the residues in the secondary coordination sphere of *Rc*FdsDABG identified three residues (H387M, R587T, and a deletion of Arg^{597}) that were able to impart nitrate reductase activity when changed to the corresponding residues in NapA.[25] The turnover rates (k_{cat}) of these individual and combination variants ranged from 0.06 min^{-1} (0.001 s^{-1}) in the case of H387M to 2.23 min^{-1} (0.037 s^{-1}) for the R587T/R-597* variant. These variants also retained significant formate dehydrogenase activity with rates that approximated the wild-type in the case of the H387M variant. It was noted that desulfo *Rc*FdsDABG, which has a terminal oxo in place of the terminal sulfido required for the hydride transfer during formate oxidation, is active to nitrate reduction at a rate of 0.31 min^{-1} (0.005 s^{-1}). We investigated the *Cn*FdsDABG for nitrate reductase activity in the as-purified enzyme and do indeed detect trace activity that varies on the enzyme purification, consistent with what was observed in the *Rc*FdsDABG homolog. Under the proposed nitrate reductase mechanism, a terminal oxo is required for catalysis, not the terminal sulfido present in the wild-type enzyme. To remove the terminal sulfido we incubated the wild-type enzyme with KCN which is known to remove the terminal sulfido to yield a terminal oxo, similar to the primary coordination sphere of nitrate reductase.[17,27,32] Following inactivation with 2 mM KCN for two hours, we observe a loss of formate dehydrogenase activity, but gain significant nitrate reductase activity compared to the inactivated *Rc*FdsDABG at a rate of 0.41 s^{-1}. This suggests that indeed the oxo, and not sulfido, form of the enzyme is needed to reduce nitrate. We attribute the varying

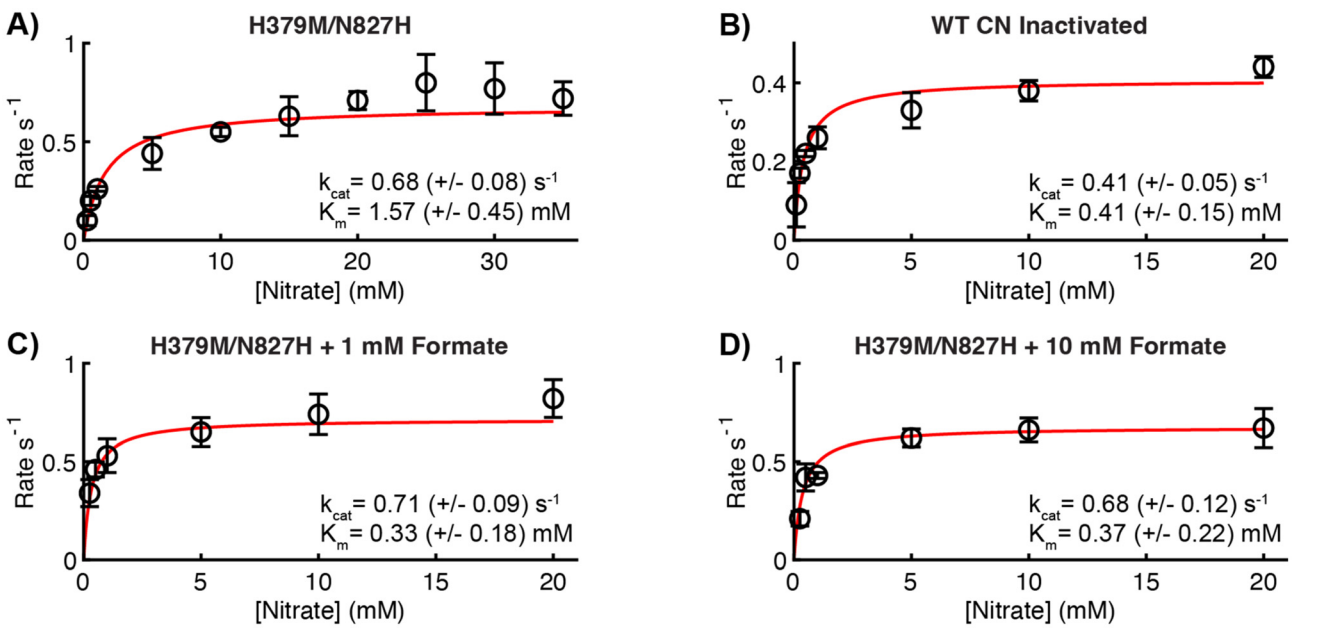

Fig. 3 Steady state kinetics of FdsDABG. Plots of the observed rate of methyl viologen cation radical (MV) consumption by FdsDABG in the presence of varying nitrate concentrations in the absence (A and B) or presence of formate (C and D). The steady state kinetics of the H379M/N827H double variant (A) can be compared against the CN inactivated wild-type (B). While both have nitrate reductase activity, the rate of the double variant is improved compared to that of the inactivated wild-type. The rates were corrected for background oxidation of MV by trace oxygen in the glovebox, enzyme functionality, and the ratio of methyl viologen oxidation to nitrate reduction (2 : 1) to reflect the rate of nitrate reduction by FdsDABG. The data was fit to a hyperbolic function (black) reflecting the Michaelis–Menten equation yielding a k_{cat} and K_m for the reaction. 95% confidence intervals of the fits are indicated.

trace nitrate reductase activity in the as-purified enzyme to some population of the desulfo enzyme, inactivated by air.[27] While the wild-type enzyme requires KCN inactivation to gain nitrate reductase activity, we observe no change in the rates of the H379M/N827H double variant suggesting the terminal ligand is present as an oxo upon purification of the double variant enzyme. We note the expression vector used here for the wild-type and double variant are the same, both possessing FdsC which sulfurates the Mo prior to the cofactor insertion into the enzyme suggesting the double variant is intrinsically less stable at the terminal ligand site and prone to exchange with water.

Our working model to rationalize these observed changes, keeping the respective proposed mechanisms for formate oxidation or nitrate reduction in mind, is that the residues highlighted here serve an important role in the stability of the terminal ligand and the resulting mechanism the enzyme facilitates, Fig. 4. We propose that the residues under investigation act as modulators to sulfur ligands of Mo. By changing the hydrogen bonding and electrostatic interactions we envision a pseudo-Jahn Teller effect where shortening of the sulfur bonds (increased bonding character) of the cysteine thiol and one of the PDT thiols, which happen to be roughly *trans* from each other in the Mo coordination sphere would then weaken the bonding interaction of the terminal ligand allowing for displacement during the oxygen atom transfer reaction that takes place for nitrate reduction. Conversely, in wild-type Fdh, the hydrogen bonding interactions allow for a more stable bonding interaction with the terminal ligand which is necessary to stabilize the terminal sulfur required for formate oxidation and CO_2 reduction *via* outer sphere hydride transfer.

To summarize, we have identified two key residues that work synergistically to direct the catalytic outcome in two highly similar molybdenum enzymes, NapA and Fdh. The double variant removes the ability of Fdh to catalyze the oxidation of formate by hydride transfer and allows for nitrate reduction by oxygen atom transfer. The oxygen atom transfer mechanism in all Mo-containing enzymes requires substrate to displace a terminal water ligand at Mo. We propose these residues impact the lability of the terminal ligand to Mo thus shifting catalysis from the outer sphere native hydride transfer to inner sphere oxygen atom transfer. Our results here highlight the importance of secondary sphere, non-covalent, interactions in tuning the MoPDT to accommodate the impressive substrate scope of Mo-containing enzymes and the intrinsic activity (oxygen atom transfer *vs.* hydride transfer) of the enzyme.

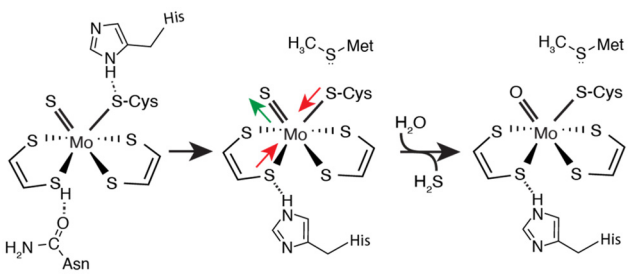

Fig. 4 A graphical summary of our hypothesis of how the hydrogen bonds between the peptide and the MoPDT interact to either stabilize or destabilize the terminal site in the case of formate dehydrogenase or nitrate reductase respectively.

Conflicts of interest

There are no conflicts to declare.

Data availability

Data from this study are available from the corresponding author upon request.

SI includes structural and sequence comaprisons of NapA and Fdh homologs, pH dependence of the steady state kinetics, and sequence information of the expression vector. See DOI: **https://doi.org/10.1039/d5dt01559f**.

Acknowledgements

We thank Prof Russ Hille (UC Riverside) for sharing the wild-type FdsDABG expression plasmid. We gratefully acknowledge financial support for this work from the UWM Office of Research (to JW).

References

1 R. Hille, J. Hall and P. Basu, The mononuclear molybdenum enzymes, *Chem. Rev.*, 2014, **114**(7), 3963–4038, DOI: **10.1021/cr400443z**. Epub 2014/01/29. PubMed PMID: 24467397; PMCID: PMC4080432.

2 S. Grimaldi, B. Schoepp-Cothenet, P. Ceccaldi, B. Guigliarelli and A. Magalon, The prokaryotic Mo/W-bisPGD enzymes family: a catalytic workhorse in bioenergetic, *Biochim. Biophys. Acta*, 2013, **1827**(8–9), 1048–1085, DOI: **10.1016/j.bbabio.2013.01.011**. PubMed PMID: 23376630.

3 Y. Lu and J. S. Valentine, Engineering metal-binding sites in proteins, *Curr. Opin. Struct. Biol.*, 1997, 7(4), 495–500, DOI: **10.1016/s0959-440x(97)80112-1**. Epub 1997/08/01. PubMed PMID: 9266170.

4 R. H. Holm and E. I. Solomon, Preface: biomimetic inorganic chemistry, *Chem. Rev.*, 2004, **104**(2), 347–348, DOI: **10.1021/cr0206364**. Epub 2004/02/12. PubMed PMID: 14871127.

5 R. L. Shook and A. S. Borovik, The effects of hydrogen bonds on metal-mediated O2 activation and related processes, *Chem. Commun.*, 2008, (46), 6095–6107, DOI: **10.1039/b810957e**. Epub 2008/12/17. PubMed PMID: 19082087; PMCID: PMC2921322.

6 R. H. Holm and E. I. Solomon, Introduction: bioinorganic enzymology II, *Chem. Rev.*, 2014, **114**(7), 3367–3368, DOI: 10.1021/cr500118g. Epub 2014/04/10. PubMed PMID: 24712923.

7 J. Liu, S. Chakraborty, P. Hosseinzadeh, Y. Yu, S. Tian, I. Petrik, A. Bhagi and Y. Lu, Metalloproteins containing cytochrome, iron-sulfur, or copper redox centers, *Chem. Rev.*, 2014, **114**(8), 4366–4469, DOI: 10.1021/cr400479b. Epub 2014/04/25. PubMed PMID: 24758379; PMCID: PMC4002152.

8 P. J. Ellis, T. Conrads, R. Hille and P. Kuhn, Crystal structure of the 100 kDa arsenite oxidase from Alcaligenes faecalis in two crystal forms at 1.64 A and 2.03 A, *Structure*, 2001, **9**(2), 125–132, DOI: 10.1016/s0969-2126(01)00566-4. Epub 2001/03/16. PubMed PMID: 11250197.

9 A. S. McAlpine, A. G. McEwan, A. L. Shaw and S. Bailey, Molybdenum active centre of DMSO reductase from Rhodobacter capsulatus: crystal structure of the oxidised enzyme at 1.82 Å resolution and the dithionite-reduced enzyme at 2.8 Å resolution, *JBIC, J. Biol. Inorg. Chem.*, 1997, **2**(6), 690–701, DOI: 10.1007/s007750050185.

10 C. Coelho, P. J. Gonzalez, J. J. G. Moura, I. Moura, J. Trincao and M. J. Romao, The Crystal Structure of Cupriavidus necator Nitrate Reductase in Oxidized and Partially Reduced States, *J. Mol. Biol.*, 2011, **408**(5), 932–948, DOI: 10.1016/j.jmb.2011.03.016. PubMed PMID: WOS:000291066200012.

11 J. M. Dias, M. E. Than, A. Humm, R. Huber, G. P. Bourenkov, H. D. Bartunik, S. Bursakov, J. Calvete, J. Caldeira, C. Carneiro, J. J. G. Moura, I. Moura and M. J. Romao, Crystal structure of the first dissimilatory nitrate reductase at 1.9 angstrom solved by MAD methods, *Structure*, 1999, **7**(1), 65–79, DOI: 10.1016/s0969-2126(99)80010-0. PubMed PMID: WOS:000079349700010.

12 S. Najmudin, P. J. Gonzalez, J. Trincao, C. Coelho, A. Mukhopadhyay, N. M. Cerqueira, C. C. Romao, I. Moura, J. J. Moura, C. D. Brondino and M. J. Romao, Periplasmic nitrate reductase revisited: a sulfur atom completes the sixth coordination of the catalytic molybdenum, *J. Biol. Inorg. Chem.*, 2008, **13**(5), 737–753, DOI: 10.1007/s00775-008-0359-6. Epub 2008/03/11. PubMed PMID: 18327621.

13 J. C. Boyington, V. N. Gladyshev, S. V. Khangulov, T. C. Stadtman and P. D. Sun, Crystal structure of formate dehydrogenase H: Catalysis involving Mo, molybdopterin, selenocysteine, and an Fe4S4 cluster, *Science*, 1997, **275**(5304), 1305–1308, DOI: 10.1126/science.275.5304.1305. PubMed PMID: WOS:A1997WK64400042.

14 H. Raaijmakers, S. Macieira, J. M. Dias, S. Teixeira, S. Bursakov, R. Huber, J. J. Moura, I. Moura and M. J. Romao, Gene sequence and the 1.8 A crystal structure of the tungsten-containing formate dehydrogenase from Desulfovibrio gigas, *Structure*, 2002, **10**(9), 1261–1272, DOI: 10.1016/s0969-2126(02)00826-2. Epub 2002/09/11. PubMed PMID: 12220497.

15 C. Radon, G. Mittelstadt, B. R. Duffus, J. Burger, T. Hartmann, T. Mielke, C. Teutloff, S. Leimkuhler and P. Wendler, Cryo-EM structures reveal intricate Fe-S cluster arrangement and charging in Rhodobacter capsulatus formate dehydrogenase, *Nat. Commun.*, 2020, **11**(1), 1912, DOI: 10.1038/s41467-020-15614-0. Epub 2020/04/22. PubMed PMID: 32313256; PMCID: PMC7171172.

16 L. B. Maia, J. J. Moura and I. Moura, Molybdenum and tungsten-dependent formate dehydrogenases, *J. Biol. Inorg. Chem.*, 2015, **20**(2), 287–309, DOI: 10.1007/s00775-014-1218-2. Epub 2014/12/06. PubMed PMID: 25476858.

17 P. Kalimuthu, S. Hakopian, D. Niks, R. Hille and P. V. Bernhardt, The Reversible Electrochemical Interconversion of Formate and CO(2) by Formate Dehydrogenase from Cupriavidus necator, *J. Phys. Chem. B*, 2023, **127**(39), 8382–8392, DOI: 10.1021/acs.jpcb.3c04652. Epub 2023/09/20. PubMed PMID: 37728992.

18 M. Meneghello, A. R. Oliveira, A. Jacq-Bailly, I. A. C. Pereira, C. Leger and V. Fourmond, Formate Dehydrogenases Reduce CO(2) Rather than HCO(3)(-) : An Electrochemical Demonstration, *Angew. Chem., Int. Ed.*, 2021, **60**(18), 9964–9967, DOI: 10.1002/anie.202101167. Epub 2021/02/19. PubMed PMID: 33599383.

19 D. Niks, J. Duvvuru, M. Escalona and R. Hille, Spectroscopic and Kinetic Properties of the Molybdenum-containing, NAD+-dependent Formate Dehydrogenase from Ralstonia eutropha, *J. Biol. Chem.*, 2016, **291**(3), 1162–1174, DOI: 10.1074/jbc.M115.688457. Epub 2015/11/11. PubMed PMID: 26553877; PMCID: PMC4714199.

20 J. Y. Yang, T. A. Kerr, X. S. Wang and J. M. Barlow, Reducing CO2 to HCO2(-) at Mild Potentials: Lessons from Formate Dehydrogenase, *J. Am. Chem. Soc.*, 2020, **142**(46), 19438–19445, DOI: 10.1021/jacs.0c07965. Epub 2020/11/04. PubMed PMID: 33141560.

21 J. Yang, B. Mintmier, K. Kc, M. C. Metzger, M. Radhakrishnan, J. McGarry, J. Wilcoxen, P. Basu and M. L. Kirk, Active Site Characterization of a Campylobacter jejuni Nitrate Reductase Variant Provides Insight into the Enzyme Mechanism, *Inorg. Chem.*, 2024, **63**(29), 13191–13196, DOI: 10.1021/acs.inorgchem.4c01991. Epub 2024/07/10. PubMed PMID: 38984973.

22 N. C. Giri, B. Mintmier, M. Radhakrishnan, J. W. Mielke, J. Wilcoxen and P. Basu, The critical role of a conserved lysine residue in periplasmic nitrate reductase catalyzed reactions, *J. Biol. Inorg. Chem.*, 2024, **29**(4), 395–405, DOI: 10.1007/s00775-024-02057-x. Epub 2024/05/24. PubMed PMID: 38782786.

23 J. McGarry, B. Mintmier, M. C. Metzger, N. C. Giri, N. Britt, P. Basu and J. Wilcoxen, Insights into periplasmic nitrate reductase function under single turnover, *J. Biol. Inorg. Chem.*, 2024, **29**(7–8), 811–819, DOI: 10.1007/s00775-024-02087-5.

24 B. Mintmier, J. M. McGarry, D. J. Bain and P. Basu, Kinetic consequences of the endogenous ligand to molybdenum in the DMSO reductase family: a case study with periplasmic nitrate reductase, *J. Biol. Inorg. Chem.*, 2021, **26**(1), 13–28, DOI: 10.1007/s00775-020-01833-9. Epub 2020/11/02. PubMed PMID: 33131003.

25 T. Hartmann, P. Schrapers, T. Utesch, M. Nimtz, Y. Rippers, H. Dau, M. A. Mroginski, M. Haumann and S. Leimkuhler, The Molybdenum Active Site of Formate Dehydrogenase Is Capable of Catalyzing C-H Bond Cleavage and Oxygen Atom Transfer Reactions, *Biochemistry*, 2016, **55**(16), 2381–2389, DOI: **10.1021/acs.biochem.6b00002**. Epub 2016/04/08. PubMed PMID: 27054466.

26 C. Coelho and M. J. Romao, Structural and mechanistic insights on nitrate reductases, *Protein Sci.*, 2015, **24**(12), 1901–1911, DOI: **10.1002/pro.2801**. Epub 2015/09/13. PubMed PMID: 26362109; PMCID: PMC4815237.

27 S. Hakopian, D. Niks and R. Hille, The air-inactivation of formate dehydrogenase FdsDABG from Cupriavidus necator, *J. Inorg. Biochem.*, 2022, **231**, 111788, DOI: **10.1016/j.jinorgbio.2022.111788**. Epub 2022/03/22. PubMed PMID: 35313132.

28 M. J. Axley and D. A. Grahame, Kinetics for formate dehydrogenase of Escherichia coli formate-hydrogenlyase, *J. Biol. Chem.*, 1991, **266**(21), 13731–13736, DOI: **10.1016/s0021-9258(18)92760-2**.

29 M. Wells, N. J. Kanmanii, A. M. Al Zadjali, J. E. Janecka, P. Basu, R. S. Oremland and J. F. Stolz, Methane, arsenic, selenium and the origins of the DMSO reductase family, *Sci. Rep.*, 2020, **10**(1), 10946, DOI: **10.1038/s41598-020-67892-9**. Epub 2020/07/04. PubMed PMID: 32616801; PMCID: PMC7331816.

30 F. Li and M. Lienemann, Stabilization of the catalytically active structure of a molybdenum-dependent formate dehydrogenase depends on a highly conserved lysine residue, *FEBS J.*, 2025, **292**(12), 2953–3265, DOI: **10.1111/febs.70048**. Epub 2025/03/03. PubMed PMID: 40028997.

31 S. G. Mayhew, The redox potential of dithionite and SO-2 from equilibrium reactions with flavodoxins, methyl viologen and hydrogen plus hydrogenase, *Eur. J. Biochem.*, 1978, **85**(2), 535–547, DOI: **10.1111/j.1432-1033.1978.tb12269.x**. Epub 1978/04/17. PubMed PMID: 648533.

32 L. B. Maia, L. Fonseca, I. Moura and J. J. Moura, Reduction of Carbon Dioxide by a Molybdenum-Containing Formate Dehydrogenase: A Kinetic and Mechanistic Study, *J. Am. Chem. Soc.*, 2016, **138**(28), 8834–8846, DOI: **10.1021/jacs.6b03941**. Epub 2016/06/28. PubMed PMID: 27348246.